

# INTERNATIONAL JOURNAL OF CHEMICAL REACTOR ENGINEERING

---

*Volume 1*

2003

*Article A12*

---

## Performance Enhancement of Photocatalytic Reactor Utilizing Flow Instability

Kanheya Mehrotra\*

Ajay Kumar Ray†

\*National University of Singapore, arun3112@rediffmail.com

†National University of Singapore, cheakr@nus.edu.sg

ISSN 1542-6580

Copyright ©2003 by the authors.

All rights reserved. No part of this publication may be reproduced, stored in a retrieval system, or transmitted, in any form or by any means, electronic, mechanical, photocopying, recording, or otherwise, without the prior written permission of the publisher, bepress, which has been given certain exclusive rights by the author.

# Performance Enhancement of Photocatalytic Reactor Utilizing Flow Instability

Kanheya Mehrotra and Ajay Kumar Ray

## Abstract

A detailed analysis has been performed for a heterogeneous photocatalytic Taylor vortex reactor that uses flow instability to recirculate fluid continually from the vicinity of the rotating inner cylindrical surface (coated with catalyst) to the stationary outer cylindrical surface of an annulus. A detailed time accurate computation when the reactor is started impulsively shows the different stages of flow evolution and the effects of finite length of the reactor in creating eddies, the overall effects of which shows very high efficiency of photocatalytic conversion. The physical arrangement considered is such that pollutant degradation is maximized by a combination of the controlled periodic illumination effect and the motion of fluid particles in a specific regime of centrifugal instability. It was found out that optimum Reynolds's number is 380 as the system reaches steady state faster, number of vortices per unit length is more, vortices move faster towards center from end, and the magnitude of both axial and radial component of velocity is more than at higher or lower value of Reynolds's number.

**KEYWORDS:** Environment, remediation, pollution, simulation, fluid mechanics, mass transfer, multiphase reactors, laminar flow, Reaction engineering

## 1. INTRODUCTION

Heterogeneous photocatalysis is one of the advanced oxidation technologies for air and water purification treatment and is documented in various references (Ollis et al., 1989; Fox and Dulay, 1993; Hoffmann et al., 1995; Hermann, 1999). This technology is based on the reactive holes and electrons generated on the surface of a semiconductor when it is illuminated by light with energy greater than its band-gap energy. These holes and electrons either recombine or become involved in redox reactions. Using this technology *in-situ* degradation of toxic compounds can be achieved both by oxidation (using photogenerated holes to oxidize organics, dyes, surfactants, pesticides, etc. (Halmann, 1995)) and by reduction (using photogenerated electrons to reduce toxic metal ions (Chen and Ray, 2001)). The appeal of this process technology is the number of advantages this process has over the traditional methods and other advanced oxidation processes of water treatment, particularly, (a) complete mineralization of almost all organic pollutants to environmentally benign effluents such as carbon dioxide, water and mineral acid, (b) in general, there is no need for use of expensive oxidizing chemicals (such as  $O_3$  or  $H_2O_2$ ) since dissolved oxygen (or air) is sufficient, (c)  $TiO_2$  as catalyst is active, inexpensive, non-hazardous, stable and reusable, and (d) the light required to activate the catalyst is low energy UV-A, and it is also possible to use solar light as an alternative (Ray and Beenackers, 1997).

In spite of the ability of this promising technology, development of a practical water treatment system has not yet been successfully achieved. There are several factors that hinder the efficient design of photocatalytic reactors (Mukherjee and Ray, 1999). Photocatalytic reactions are complex multi-phase reaction system. The solid photocatalyst is distributed within the continuous fluid phase, water and oxygen (or air) and the UV-light electronic phase. In this type of reactors, besides conventional reactor problems such as reactant-catalyst contacting, flow patterns, mixing, mass transfer, reaction kinetics, catalyst installation, temperature control etc., an added engineering aspect related to illumination of catalyst becomes important. The illumination issue is of extreme importance since the amount of catalyst that can be activated determines the water treatment capacity of the reactor. The extent of interface among the transport processes, reaction kinetics and light absorption leads to a strong combination of physico-chemical phenomena and it is one of the major barrier in the technical development of a photocatalytic reactor.

The scale-up of fixed-bed photocatalytic reactor has been severely limited as reactor configurations have not been able to address the issue of mass transfer of pollutants to the catalyst surface. The new reactor design concepts must focus on this challenge. Earlier experimental studies of our group on catalyst coated tube bundles (Ray, 1999), novel immersion type lamps (Ray and Beenackers, 1998), and rotating tube bundles revealed that photocatalytic reaction is primarily diffusion (mass-transfer) controlled. The reaction occurs at the fluid-catalyst interface, and in most cases, the overall rate of reaction is limited to mass transport of the pollutant to the catalyst surface. In our earlier studies, we have enhanced mass transfer by increasing mixing of fluids through turbulence and introduction of baffles (Periyathamby and Ray, 1999). In this work, a new photocatalytic reactor is considered that uses flow instability to increase reaction yield throughout the reactor volume.

## 2. CENTRIFUGAL INSTABILITY OF ROTATING TAYLOR-COUETTE FLOW

The laminar flow confined within the annulus region between two co-axial cylinders with the inner one differentially rotating with respect to the outer suffers centrifugal instability depending on the geometry and rotation rates. First experimental reporting was done by Taylor (1923), although the first criteria of centrifugal instability was enunciated earlier by Rayleigh (1920), who showed that an inviscid rotating flow to be unstable, if the energy of rotation associated with fluid particle decreases radially outward. Under such unstable configuration one notices the appearance of circumferential toroidal vortices in between the two cylinders and is known as Taylor-Couette vortices. These vortices evolve due to the adverse gradient of angular momentum that creates potential unstable arrangement of flow (Chandrasekhar, 1961). Such an unstable condition arises naturally if the outer cylinder is held stationary while the inner cylinder is rotated at a sufficiently high rotation rate- an arrangement considered in the present study. A schematic of the system is shown in Fig. 1. The toroidal vortices that are formed in the annular region between the cylinders

for a particular combination of the geometric arrangement and the inner cylinder rotation rates are shown in Fig. 2(a). The non-wavy vortex flow is seen to appear as a consequence of primary instability as given by appropriate non-dimensional numbers like Taylor number and Reynolds number. When the Reynolds number is increased to somewhat higher values, then one sees the wavy vortex flow, also shown in Fig. 2(a). In such an unstable condition the annulus is filled with pair of counter rotating vortices. This can be viewed in Fig. 2(b) and 2(c). Fig. 2(c) also shows the boundary layer forming on the inner surface to have an axial periodicity. The boundary layer oscillates periodically between almost zero thickness to a maxima in between the counter-rotating vortex pair, where the two shear layers approaching each other spews out a jet of fluid towards the outer wall. The fluid particles in their motion around the toroidal vortices come periodically in contact with the inner surface. By assuming the annular gap,  $d$  [ $\equiv (r_o - r_i)$ ], as small compared to the inner cylinder radius ( $r_i$ ), where  $r_o$  is the outer cylinder radius, it has been shown by Taylor (1923) that stability is dependent only on the ratio of the rotation rate of the outer cylinder to the rotation rate of the inner cylinder,  $(\Omega_o/\Omega_i)$ , and a single parameter, called Taylor number,  $T_a$ , which can be defined as follows

$$Ta = \frac{r_i d^3 [\Omega_i^2 - \Omega_o^2]}{\nu^2} \quad (1)$$

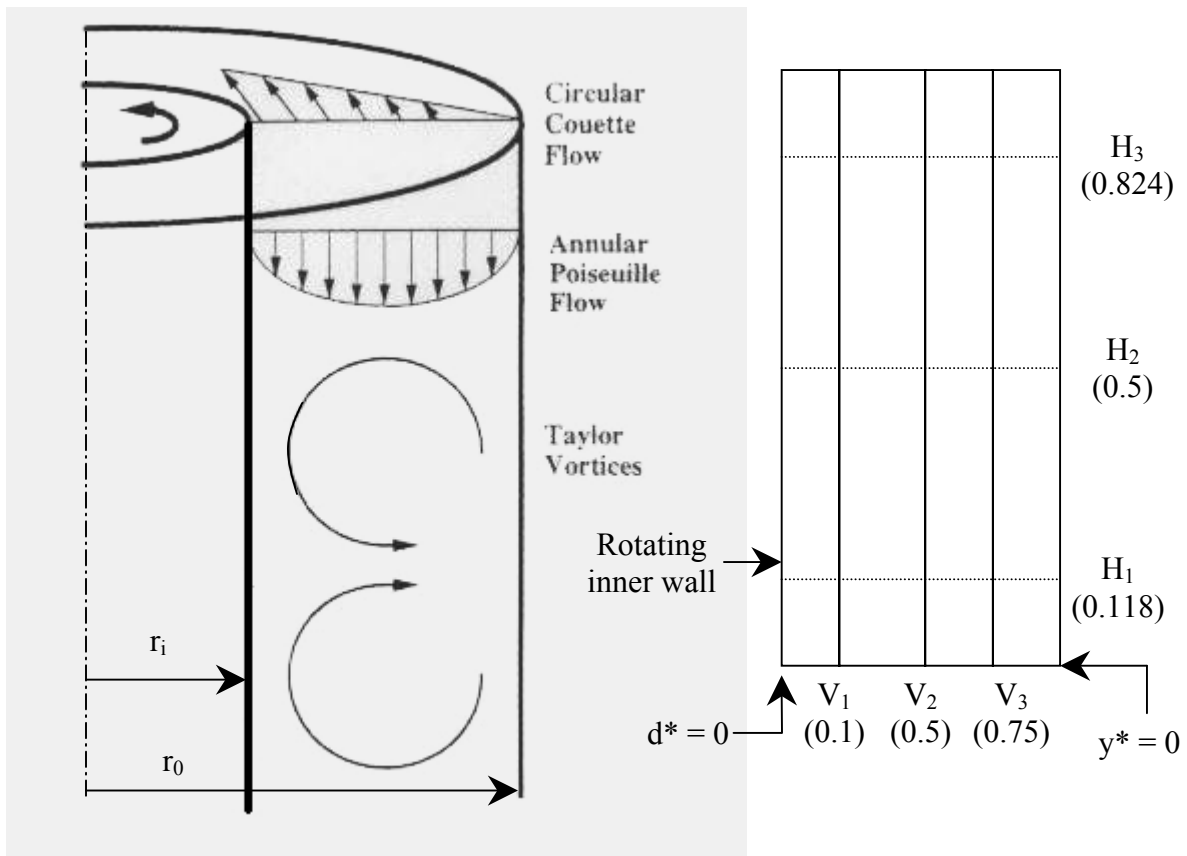


Fig. 1a

Fig. 1b

Fig. 1. (a) Schematic diagram of the Taylor vortex reactor, and (b) Location of the observation stations in the annular region to analyze flow behavior.  $d^* = 0$  (rotating inner cylinder),  $d^* = 1$  (stationary outer wall),  $y^* = 0$  (bottom),  $y^* = 1$  (top).

From the stability theory for  $0 \leq \Omega_o/\Omega_i \leq 1$  and large aspect ratio it has been established that primary instability in the form of the appearance of Taylor vortices occurs at  $Ta_{crit} \approx 1708$ . It should be noted that when outer cylinder is stationary,  $Ta$  number becomes

$$Ta = Re^2 \left[ \frac{d}{r_i} \right] \tag{2}$$

where Reynolds number,  $Re$  is given by

$$Re = \frac{d(\Omega_i r_i) \rho}{\mu} \tag{3}$$

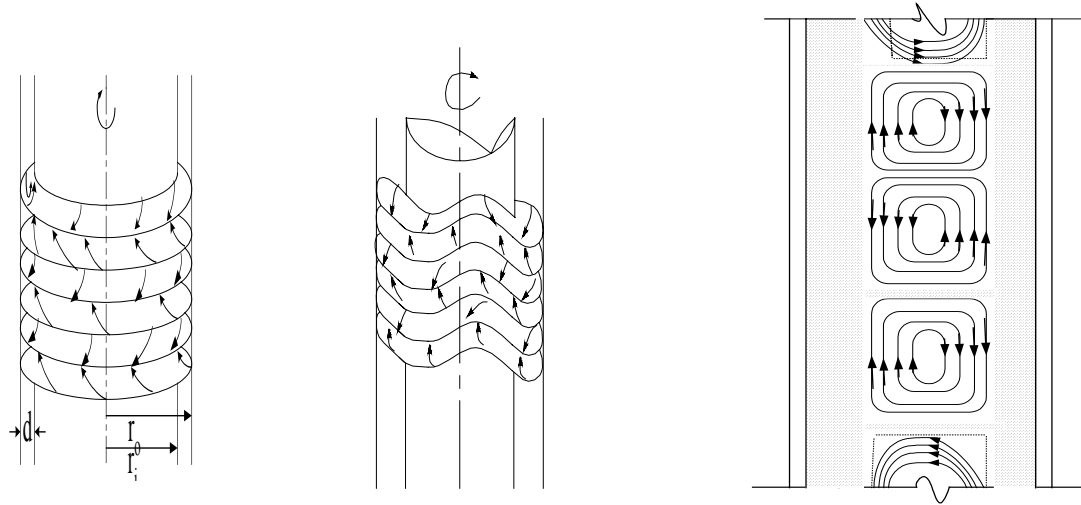


Fig. 2(a)

Fig. 2(b)

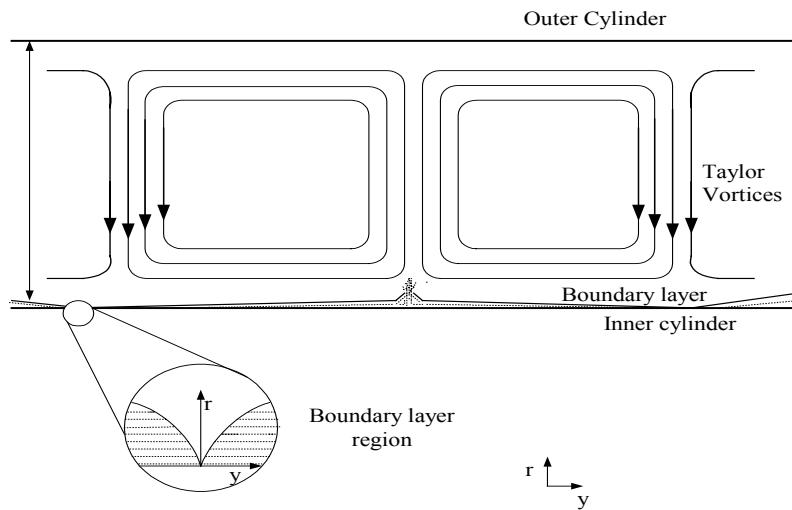


Fig. 2(c)

Fig. 2. (a) Vortices without and with circumferential waves, (b) schematic presentation of streamlines in vortical cells, and (c) radial mass transfer in Taylor-Couette flow.

Particle image velocimetry (PIV) was used to measure the axial and radial velocities in a meridional plane for non-wavy and wavy Taylor-Couette flow in the annulus between a rotating inner cylinder and a fixed outer cylinder with fixed end conditions by Wereley and Lueptow (1998). It was shown that the vortices became stronger and the outflow between pairs of vortices was jet-like. Wavy vortex flow is characterized by azimuthal deformation of vortices both axially and radially. According to their findings, it was also shown that significant transfer of fluid between neighboring vortices occurs in a cyclic fashion at certain points along an azimuthal wave so that while one vortex grows in size, the two adjacent vortices become smaller, and vice versa. Vortex cells were not independent as the significant transfer of fluid between adjacent vortices occurs in wavy flow regime. This aspect of the flow is important, because traditionally it is assumed that the vortex pair in Taylor-Couette vortices is independent of each other and is of same size and it is customary to treat this as plug flow. But, the observation of Wereley and Lueptow (1998) is significant from the point of view of present application. If indeed there is significant mass transfer between adjacent vortex pair, then that can be used for additional benefit for the performance enhancement of the present reactor. The transfer of fluid particles between adjacent vortices occurs with a cyclic fashion as a particular vortex gains fluid from adjacent vortices. It has also been reported that the degree of transfer of fluid is greater at Reynolds number equal to 253 than at either higher or lower Reynolds number. In addition to flow into and out of adjacent vortices taking place periodically, the individual vortex centers also move both axially and radially in a cyclic fashion. Once again the maximum departure in the radial direction is a strong function of Reynolds number and is found to be maximum for Re equal to 253.

Table 1. Geometric dimensions and conditions used for different simulation runs.

Specification	Case 1	Case 2	Case 3
Length L, cm	42.5	42.5	42.5
Inner radius $r_i$ , cm	4.34	4.34	4.34
Outer radius $r_o$ , cm	5.23	5.23	5.23
Annular gap, d, cm	0.89	0.89	0.89
Aspect ratio, L/d	47.70	47.70	47.70
Rotation speed, $\Omega$ , rad/s (rpm)	0.655 (6.25)	0.984 (9.39)	1.638 (15.65)
Volume of liquid treated, $V_L$ litre	1.136	1.136	1.136
Reynolds Number, Re	253	380	633
Taylor Number, Ta	13,126	29,625	50,116

In this work we have considered a Taylor Vortex Photocatalytic (TVR) reactor, which is shown schematically in figure 1 and dimension of the reactor is given in Table 1. In the present reactor it is assumed that the outer surface of the inner cylinder is coated with  $\text{TiO}_2$  photocatalyst and it is illuminated with a lamp placed inside the inner cylinder. Szechowski et al. (1995) have reported their experimental studies related to enhancing the photo-efficiency of a Taylor Vortex Reactor (TVR). But, they have used semiconductor photocatalyst particles as slurry in the fluid within the annulus. They have found that despite the photocatalyst being dispersed in the fluid, the useful reaction took place only periodically when the fluid was in contact with the illuminated inner cylinder surface. They reported three-fold increase in the photo-efficiency when the reactant was illuminated for less than 150 ms, and it stayed in dark for more than 1 s. The maximum photo-efficiency achieved by them was 30% at 300 rpm of the inner cylinder when 10 g/l loading of  $\text{TiO}_2$  was used. The major problem of achieving higher photo-efficiency was related to the transport of purified fluid from the vicinity of the catalyst. Furthermore, their configuration suffers from the additional problem of separation of sub-micron size catalyst particles after the purification stage. Moreover, the working fluid is optically dense, and therefore, the light penetration depth is restricted to a distance that is of the order of the boundary layer thickness of the inner cylinder. In view of all these factors we have considered a TVR of similar geometry, but instead of a slurry type reactor, the photocatalyst was assumed to be immobilized (fixed) on the outer surface of the inner cylinder and a fluorescent lamp illuminates the inner cylinder on which the catalyst is immobilized, and in the presence of light the catalyst is activated and as a result the redox reaction takes place. Thus, one can use a very low level of catalyst loading, and simultaneously, eliminate the process of separation of catalyst particles after the purification stage. The enhanced purification has been obtained by utilizing fluid dynamical instability associated with centrifugal

instability in the cylindrical annular geometry. It is, therefore, essential to focus on the twin aspects, photocatalysis and centrifugal instability, in an annular cylindrical geometry. The residence time in the illuminated region is a function of the angular velocity of the re-circulating vortex as well as the size of the vortex. The latter, once again depends on the gap size and the number of vortices formed in a given length of the reactor. The two most important factors for unstable Taylor-Couette flow establishment are the aspect ratio ( $L/D$ ) and the Reynolds number. The effect of aspect ratio on the flow development has been studied by Sengupta et al. (2001). In the present study we investigated the effect of Reynolds number on the formation of vortices and its effect on overall degradation of a pollutant.

### 3. THEORETICAL MODEL AND REACTOR SIMULATION

The performances of the reactor depends on the photo-efficiency of the photocatalytic process as well as on the mass transfer efficiency of the fluid from the vicinity of the rotating inner cylinder to the stationary outer cylinder and back within a single Taylor-Couette vortex. The latter depends on the primary instability of flow in setting-up of the vortical roles. This instability and associated mass transfer can be made more effective by initiating a secondary motion when additional mass transfer between neighboring roles through the wavy vortex flow would take place. This has been shown to be a strong function of Reynolds number by Werely and Lueptow (1998) and it was reported that inter-role mass transfer is maximum for the chosen geometry in their experiment for  $Re = 253$ . In the present set of computations, same geometric parameters are chosen including the aspect ratio, ( $AR = L/d$ ) of the reactor. However, in the experiment the starting protocol of the inner cylinder rotation was taken as quasi-static and the reported results were recorded after allowing the flow to develop further for 10 minutes after the attainment of the final rotation rate. In the present computations the flow is started impulsively, because for the practical operation of the reactor in a shortest possible time period. For such an operation the transient mass transfer depends strongly upon the vortices that are formed at initial times near the fixed end-caps of the reactor.

Since the rotating inner cylinder drives the flow inside the reactor and the rotation rates are low, it is quite adequate to consider the flow to be incompressible and solve the governing Navier-Stokes equation in primitive variable form as,

$$\frac{\partial \vec{V}}{\partial t} + (\vec{V} \cdot \nabla) \vec{V} = -\frac{1}{\rho} \nabla p + \nu \nabla^2 \vec{V} \quad (4)$$

and

$$\nabla \cdot \vec{V} = 0 \quad (5)$$

Furthermore, isothermal condition can be assumed for both the flow evolution and chemical reaction calculations since the pollutant being oxidized into other products is present in trace amount, and heat of reaction in photocatalytic reactions is usually negligible (Chen et al., 2000). The boundary conditions that are applied on the inner and outer cylindrical surface correspond to no-slip conditions. The end caps are considered to be a part of the outer cylinder and hence are stationary. The following boundary conditions are used for the numerical simulations. With reference to Fig. 1, on the inner cylinder surface,

$$r = r_i: V_r = V_y = 0 \quad \text{and} \quad V_\theta = \Omega_i r_i \quad (6a)$$

where  $\Omega_i(t)$  is the instantaneous rotation rate of the inner cylinder. On the outer cylinder ( $r = r_o$ ) and the end-caps ( $y = 0$  and  $L$ ):

$$V_r = V_y = V_\theta = 0 \quad (6b)$$

Since the simulation is for the impulsive start of the rotation rate of the inner cylinder,

$$t \leq 0: \quad \Omega_i(t) = 0 \quad (7a)$$

$$t > 0: \quad \Omega_i(t) = \Omega \quad (7b)$$

The model pollutant considered in this work is benzoic acid with initial concentration of 100 ppm while the initial mass fraction of  $O_2$  is taken to be equal to twice the stoichiometric requirement for the reaction given by



The rate expression for photocatalytic degradation for benzoic acid used in this study is given by (Mehrotra et al., 2002)

$$R = -\frac{dC_s}{dt} = k(I) \left[ \frac{K_s C_s}{1 + K_s C_s} \right] \quad (9)$$

where  $C_s$  is the concentration of benzoic acid at the catalyst surface,  $k(I) = 3.9 \times 10^{-4} [I]^\beta \text{ mM s}^{-1}$ ,  $\beta = 0.59$ ,  $K_s = 5.67 \text{ mM}^{-1}$ . In the expression for  $k(I)$ , unit of intensity,  $I$  is in  $\text{W/m}^2$ , and the exponent  $\beta$  was obtained from least square fit of the experimental results of  $k$  (in  $\text{mM/s}$ ) against  $I$  (in  $\text{W/m}^2$ ). Note that the initial concentration of the pollutant is considered to 100 ppm, which slightly on the higher side in order to observe noticeable changes in the contour plot of photocatalytic degradation of benzoic acid from the simulation run as simulation runs are quite expensive and time consuming as discussed later. Benzoic acid is selected as the model component for two reasons. Firstly, true kinetic data were available from our earlier studies (Mehrotra et al., 2002) and secondly, it is possible to be monitored on-line easily by a spectrophotometer. The amount of catalyst coating is assumed to be  $0.3 \text{ mg/cm}^2$ , which is easily achievable using our dip-coating apparatus (Ray and Beenackers, 1998). The density of the system is assumed to be constant and equal to that of water as the pollutant is present at very low concentration.

#### 4. COMPUTATIONAL DETAILS

In computing the flow, the three-dimensional Navier-Stokes equation is solved in primitive formulation by using the commercial software Fluent<sup>®</sup>. This is found adequate as the flow considered is laminar, and therefore, the need for resolving large ranges of wave numbers and circular frequencies is not necessary. In solving the governing equations no simplification is made regarding symmetry and reflection of the solution. The time-accurate solution was obtained instead of assuming a priori steady state. The geometric dimensions chosen for the reactor is identical to the value reported in Werely and Lueptow (1998). The reactor is considered to be operating in a batch mode, purifying 1.136 litre of water at a time. Three different rotation speed of the inner cylinder is considered 0.655, 0.984 and 1.638 rad/s, which result in Reynolds numbers,  $Re$ , of 253, 380 and 633 respectively. The rotation speed is varied to obtain Reynolds number respectively 1.5 and 2.5 times that of the first case ( $Re = 253$ ). The present reactor provides  $0.116 \text{ m}^2$  of illuminated catalyst surface area and illuminated catalyst density of  $102 \text{ m}^2/\text{m}^3$ .

For generating grids within the annulus region of the geometry, every edge in three directions is defined with certain nodes. There are high shear regions near the inner cylinder wall, the outer cylinder wall and the end cap regions. Therefore, axial and radial derivatives of all physical variables across such layers would be larger than in the azimuthal direction, and consequently, more grid points are taken in axial and radial directions compared to azimuthal direction. In order to incorporate these, grid points are taken more clustered in two ends and next to inner and outer wall. To enhance the direct mapping of grid from upper wall to bottom wall, the total geometry is separated into two volumes by a brick. Two interior planes are created by this process within the annular space that was used to analyze our results at the time of post processing. Grid points along the three directions are taken as follows:  $r \times \theta \times h = 100 \times 40 \times 75$ . Fluent pre-processor GAMBIT<sup>®</sup> 1.1 is used to create geometry and generate grid for both cases. There are 0.3 million cells, 907,000 total quadrilateral faces (3,000 inner wall faces, 11,000 outer wall spaces, 15,000 interior plane faces and 878,000 rest of interior plane faces). The total numbers of nodes are 307,040. The present set of computation of Navier-Stokes equation for Taylor-Couette geometry is expensive. The one without reaction was computed in 1.5Gb RAM Windows NT workstation and it took 78 hours of actual time for simulation results of 10s.

The equations (4) and (5) are solved subject to the boundary conditions and initial conditions defined in equations (6) and (7) within the annulus between the cylinders as shown in Fig. 1(a). The results are shown in Fig. 3, in the radial-axial ( $r$ - $y$ ) plane and along the three sets of horizontal ( $H_1$ - $H_3$ ) as well as vertical lines ( $V_1$ - $V_3$ ) as indicated in Fig. 1.

A brief description of the method is given below. The solver is based on solving equations (4) and (5) in a sequential manner by a control volume based technique using the following three steps. Firstly, the computing domain was discretized into discrete control volume using a computational grid. The governing equations were time advanced in integral form for each computational cell to yield algebraic equations for the discrete dependent variables, such as velocity components, pressure and conserved scalars. Finally, the discrete equations were linearized into a set of algebraic equations, which were solved to yield updated

variables. For the discretization process, the familiar QUICK scheme was used for the momentum and species equations, as this is a higher-order accurate scheme with minimum numerical dissipation that is implicit with the discretization. The solver uses finite volume method in solving the Navier-Stokes equation.

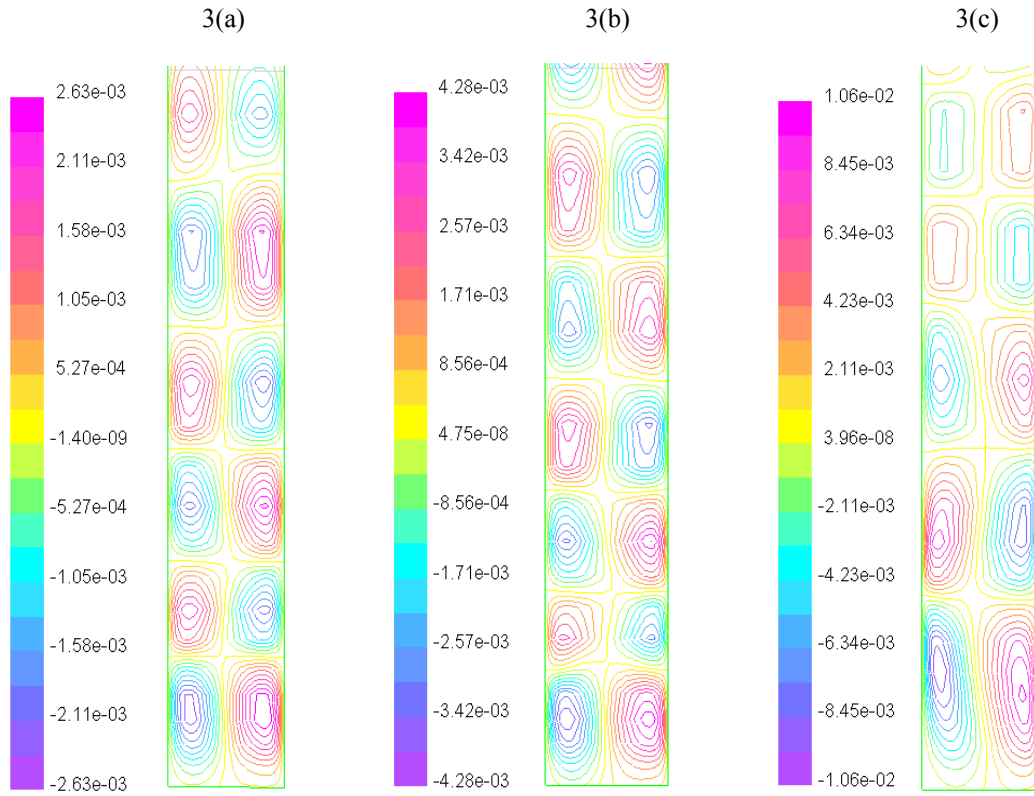


Fig. 3. Contours of axial velocity between  $y^* = 0$  (bottom) and  $0.1178$  (top) at  $t = 30s$  for the three different Reynolds number, (a) 253, (b) 380, and (c) 633. The right boundary is the rotating inner cylinder.

## 5. RESULTS AND DISCUSSIONS

The following non-dimensionalization is used in order to be able to compare results to reported results in literature. The annulus gap,  $d$ , is used as length scale while the speed ( $\Omega r_i$ ) imposed on the inner cylinder surface is used as the velocity scale. Thus, the dimensionless time scale used is  $t^* [\equiv t (\Omega r_i)/d]$ . Since pollutant is present as trace quantity, it is expected that the chemical reaction will not influence the fluid dynamic behavior of the system. To show this two sets of computations were initiated from  $t = 0$ , one with the chemical reaction, while in the other only the fluid flow was computed and the results compared. It was observed that flow field was identical.

In Fig. 3 the contours of the axial velocity in the annular region of 11.8% from the bottom of the reactor are shown for three different Reynolds number. The purpose of this is to compare the vortex profile when Reynolds number is varied and to elucidate the effect of Reynolds number on the flow establishment. The numbers of vortices formed for the three cases (see Table 1) are 5.75, 6.5 and 5.0 for case 1 (Fig. 3a), case 2 (Fig. 3b), and case 3 (Fig. 3c) respectively. It can be clearly seen that the number of vortices formed are maximum when the Reynolds number is 1.5 times ( $Re = 380$ ) compared to the reference case ( $Re = 253$ ). Moreover, when  $Re$  is 2.5 times that of the reference case, we see that the flow has not been completely established in the entire region. The vortex at the top is degenerated and the vortices in the middle section are also not as compact compared to the other cases. We observed the following for case 2 compared to case 1 (reference case) and case 3: (a) It reaches steady state faster, (b) number of vortices per unit length is more, (c) vortices move faster towards center from the two ends, and (d) the intensity (i.e.,

magnitude) of both axial and radial component of velocity is more than the reference case (i.e.,  $Re = 253$ ). It can be observed that for the simulated case in this work with impulsive start the optimum  $Re$  is somewhere around 380 instead of 253 as was found by Werely and Lueptow (1998). The deviation from the experimental results probably is due to the impulsive start of the simulated reactor as opposed to the quasi-static start in the experimental case. Since the case 2 gives better results (based on the four aspects mentioned above) than the other two cases, for all subsequent reported results comparison were made between the cases 1 and 2.

In Fig. 4, the axial velocity as a function of dimensionless radial coordinate is plotted for various time instants at the observation stations  $H_1$ ,  $H_2$  and  $H_3$ . When the velocity profile for cases 1 and 2 are compared, it was observed that the velocity magnitudes are 1.3 times higher (see Fig. 4a) for case 2 than that for the reference case. The results from Fig. 4a also indicate that for case 2, the rate of change of axial velocity is almost negligible and therefore, the flow reaches steady state faster than that of the reference case. From Fig. 4b, the axial velocities demonstrate that Taylor-Couette vortices move faster toward the middle part when the  $Re$  is higher. In general for both cases, since the middle section is at the centre ( $y^* = 0.5$ ), there the axial velocity is smallest in magnitude (about 4 order of magnitude lower as seen in Fig. 4b) compared to the other two observation stations. Similar conclusions can be obtained from Fig. 4c (like Fig. 4a) when compared to Fig. 4b.

Similarly, in Fig. 5, the radial component of velocity is plotted in the annular gap at the three different heights at three different non-dimensional times. Fig. 5a and 5c shows that for case 2 an inflow of fluid towards the inner cylinder for all the indicated times, while for case 1 up to  $t^* = 862$  the fluid moves towards the inner cylinder, but at  $t^* = 1581$  the fluid moves toward the outer cylinder. The rate of change of radial velocity is much slower for case 2 than for case 1, indicating the flow will reach steady state faster when  $Re = 380$ . Once again from Fig. 5b, the magnitude of the radial velocities is the smallest for both cases compared to the profiles away from the center. Fig. 5b also indicates that the flow does not show the formation of Taylor-Couette vortices in the middle part of the reactor for the reference case, but for case 2 the vortices have started forming in the center. Thus higher  $Re$  is responsible for formation of vortices at the middle part of the reactor.

In Fig. 6, axial velocity is plotted along the dimensionless axial direction at observation stations  $V_1$ ,  $V_2$  and  $V_3$ . For both the cases at smaller times, the Taylor-Couette vortices are formed at the ends and as time progresses more and more of these are formed covering the middle part. The magnitude of both axial and radial velocities is on an average 1.5 times larger for case 2 than for the reference case. From the figures 6 and 7, it is evident that for at higher  $Re$  the vortices move faster to the middle part. This is of great importance as the faster movement and formation of vortices in the entire reactor is the basis for improvement of performance of the photocatalytic Taylor vortex reactor. Of specific interest is the plot of the axial velocities in the middle of the annulus at  $V_2$ . If indeed the vortices formed were like a plug flow then this velocity component along this line would have been zero. The very fact that the velocity component alternates in sign is indicative of the fact that the vortex centres not only execute axial waviness, but also shows significant radial motion. Werely and Lueptow (1998) also observed this experimentally where they showed such motions for all Reynolds numbers between 131 to 1221. They reported large excursions of axial motions for low Reynolds numbers while maximum radial motion of vortex centres were observed for  $Re = 253$  as opposed to at  $Re = 380$  in this present case. However, it has to be noted that in the present investigation the flow is started impulsively and not accelerated quasi-statically.

In Fig. 8, the velocity vector plots are shown for only the top half of the reactor ( $y^* = 0.5 - 1.0$ ) in a given  $y - r$  plane at  $t^* = 879$  when steady state has reached. One can see weak vortices forming near the upper part of the left segment. There are regions along the height where one can see a jet-like flow starting from the inner wall moving towards the outer wall due to centrifugal action. In the segment between  $y^* = 0.7$  and  $0.85$ , significant mixing of fluid is noticeable due to the formation of coherent vortices. Once again one can see the jet-like flow from inner to outer cylinder - although the trajectory of the fluid particles are not strictly straight. Moreover, there is no visible wall shear layer forming on the inner wall as has been shown in Fig. 2(c). In the segment between 85% and the top of the reactor, the velocity vectors clearly shows recirculating rolls, although the axial lengths vary significantly due to end-wall effects. Also in this segment, apart from the jet-like regions, one can as well see small axial regions where a flow is established from the outer to the inner wall side. However, this cannot cover the entire radial gap because of centrifugal force acting on fluid particles near the inner wall. For the same reasons one will not see a wall shear layer forming on the inner cylinder as has been shown in the sketch of Fig. 2(c). Instead one would notice the

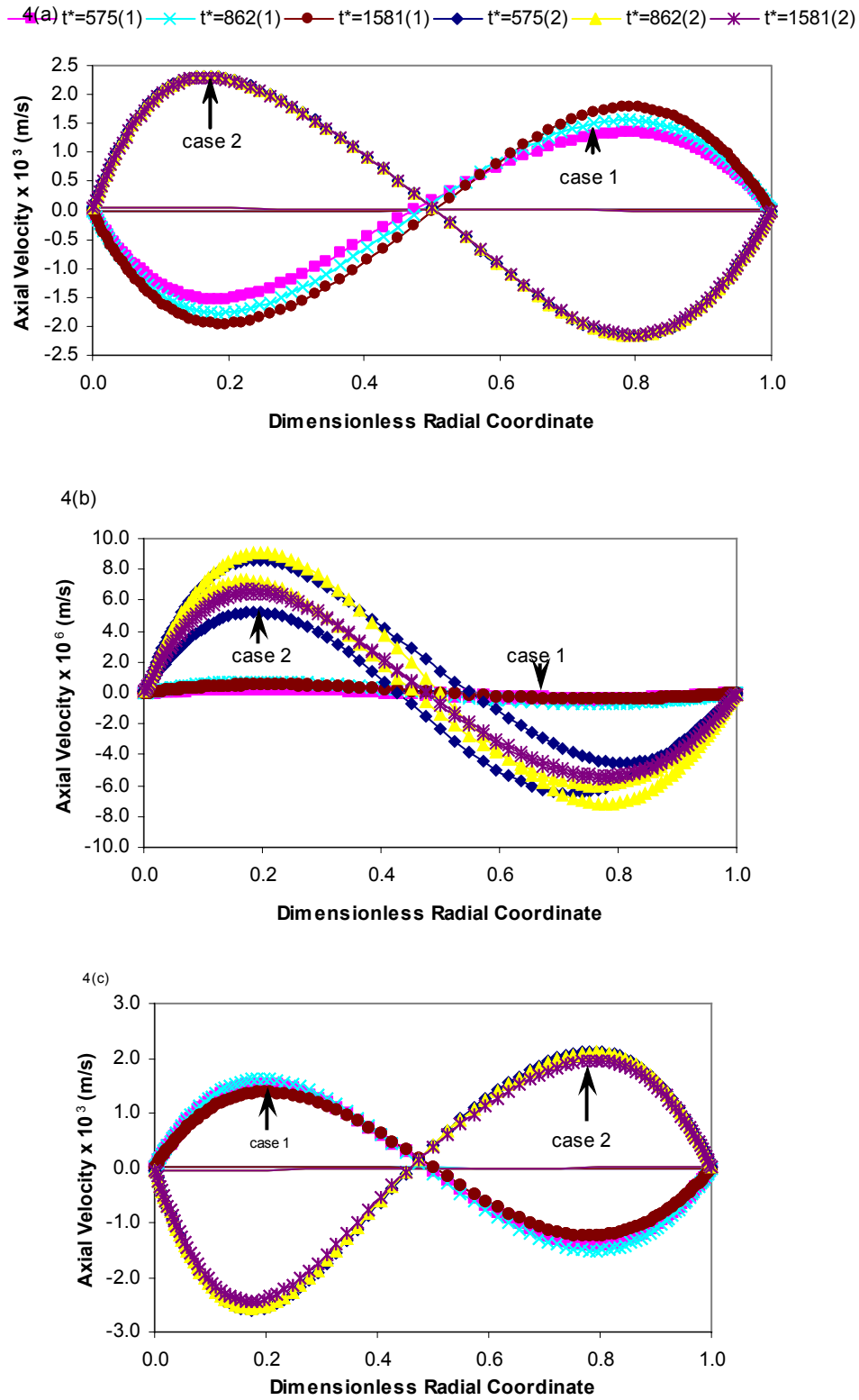


Fig. 4. Change of axial velocity with dimensionless radial coordinate at different horizontal positions and times. (a)  $H_1$ , (b)  $H_2$ , and (c)  $H_3$  for  $Re = 253$  and  $380$ .

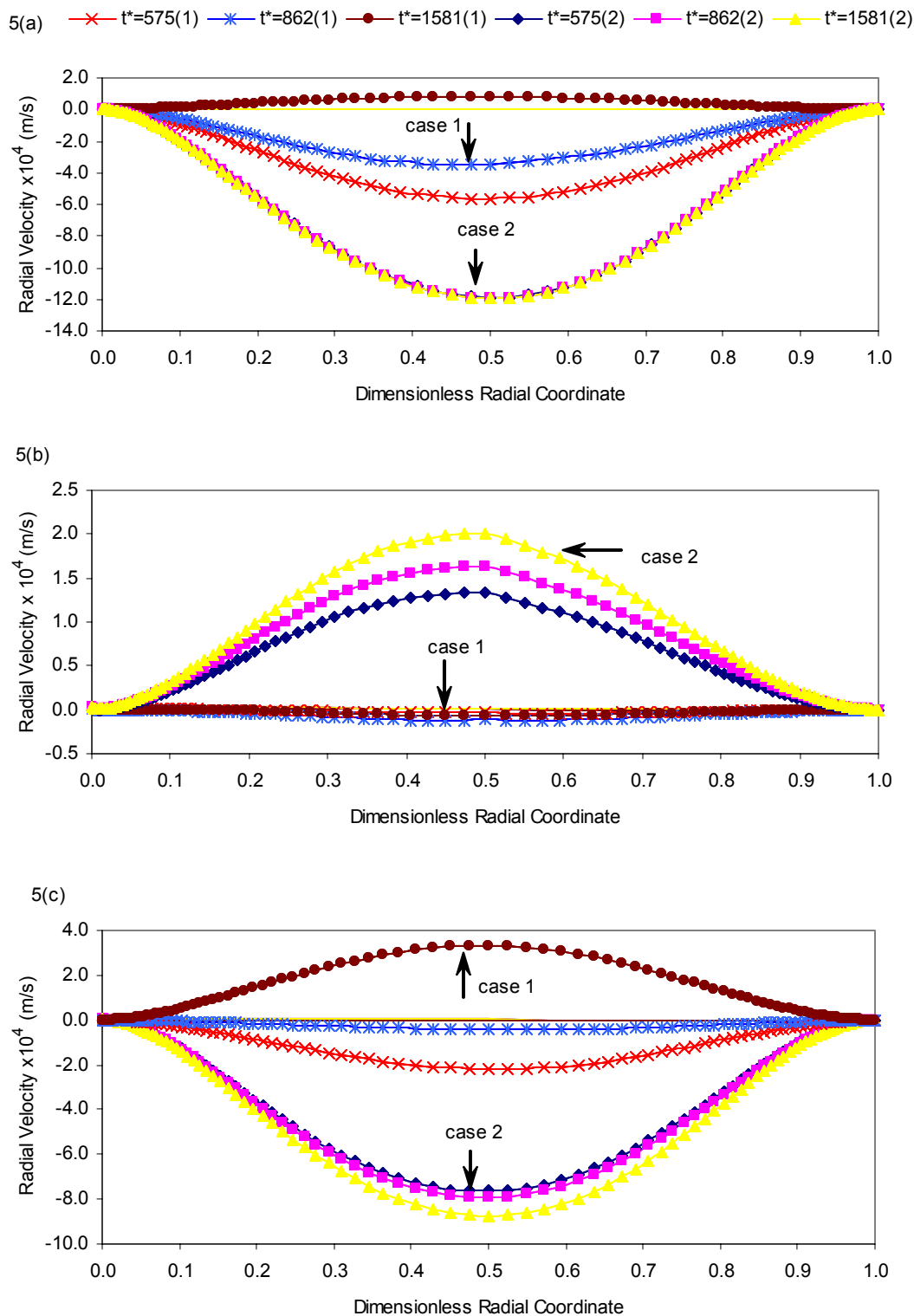


Fig. 5. Change of radial velocity with dimensionless radial coordinate at different horizontal positions and times. (a)  $H_1$ , (b)  $H_2$ , and (c)  $H_3$  for  $Re = 253$  and  $380$ .

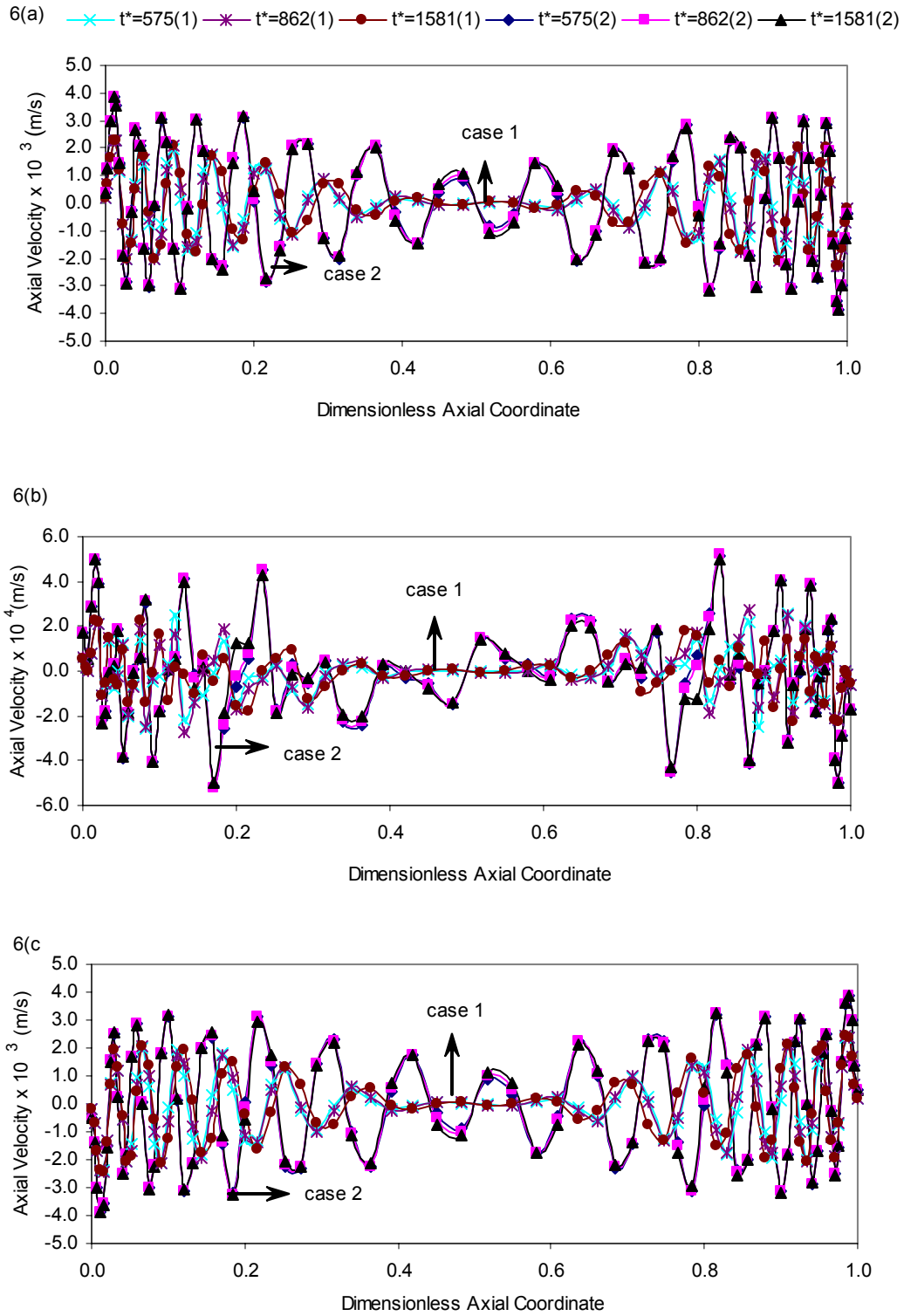


Fig. 6. Change of axial velocity with dimensionless axial coordinate at different vertical positions and times. (a)  $V_1$ , (b)  $V_2$ , and (c)  $V_3$  for  $Re = 253$  and  $380$ .

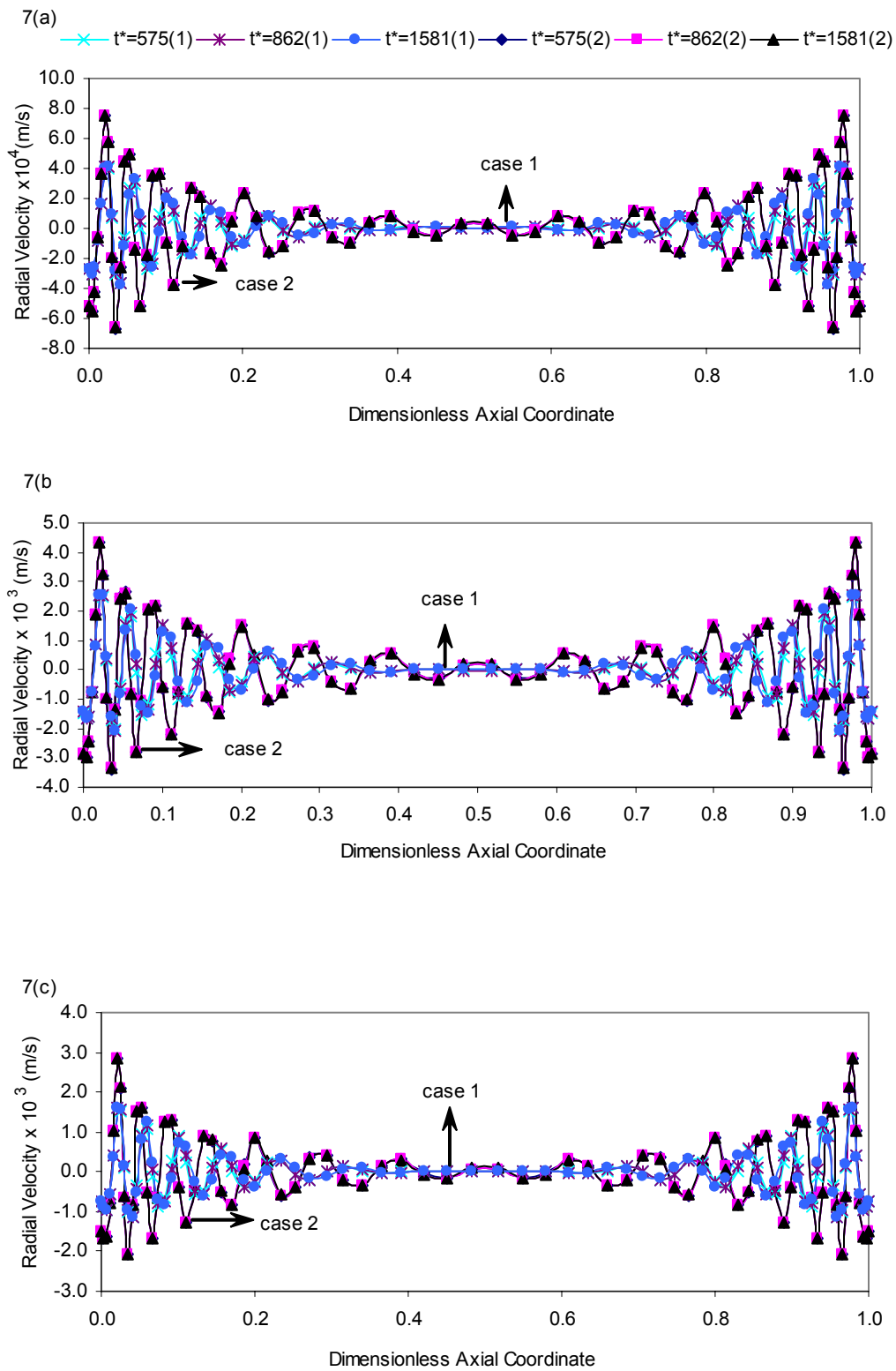


Fig. 7. Change of radial velocity with dimensionless axial coordinate at different vertical positions and times. (a)  $V_1$ , (b)  $V_2$ , and (c)  $V_3$  for  $Re = 253$  and  $380$ .

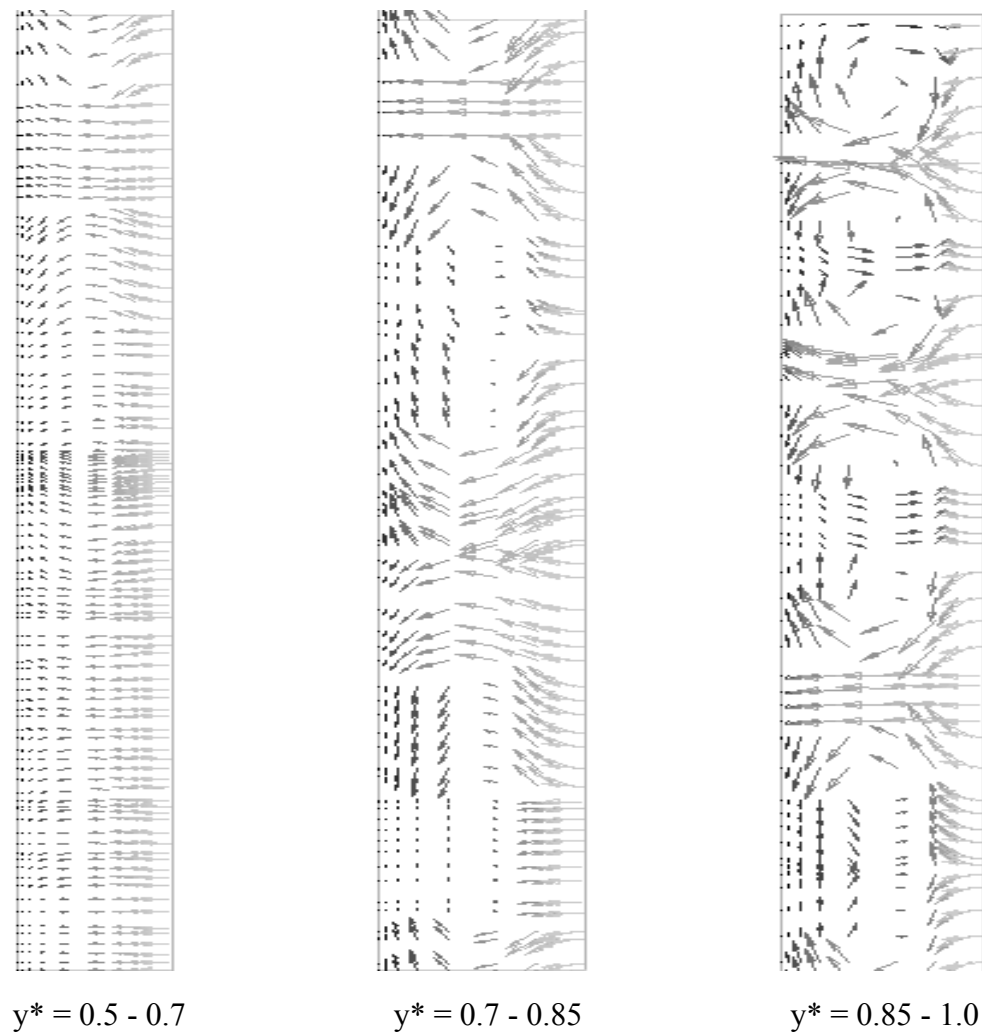


Fig. 8. Velocity vectors shown in radial plane respectively between  $y^* = 0.5 - 0.7$ ,  $y^* = 0.7 - 0.85$  and  $y^* = 0.85 - 1.0$  at  $t^* = 879s$  for  $Re = 253$ . Right side indicates rotating inner wall ( $d^* = 0$ ).

formation of an internal layer after sometime and associated full saddle point inside the flow domain. In retrospect, it appears that to resolve such internal layers, one should have finer grid in the interior too. This is shown in Fig. 9, where the velocity vectors are plotted over a limited segment between 85.5% and 88.5% of the reactor length. An internal band characterizes the formation of the internal layer where the flow is along the axis of the reactor. This is seen to originate at the saddle points, one of which is marked in the figures with filled circle for different times. The flow is seen to be axial in opposite direction across the saddle point. Such vertical lines are nothing but the internal layer. While at  $t^* = 383$ , no such inner layers were seen, it is seen for the plot shown at  $t^* = 575$ . Once this saddle point is seen to form it does not seem to move as it can be traced at the same location at later times. It is also interesting to note in Fig. 9 that between  $t^* = 671$  and  $t^* = 767$ , while the saddle point remains fixed, the velocity vectors indicate an increase in upward velocity above the saddle point while it decreases in downward direction. The velocity vectors inside the recirculating eddies show time dependent behavior, though it is not so pronounced near

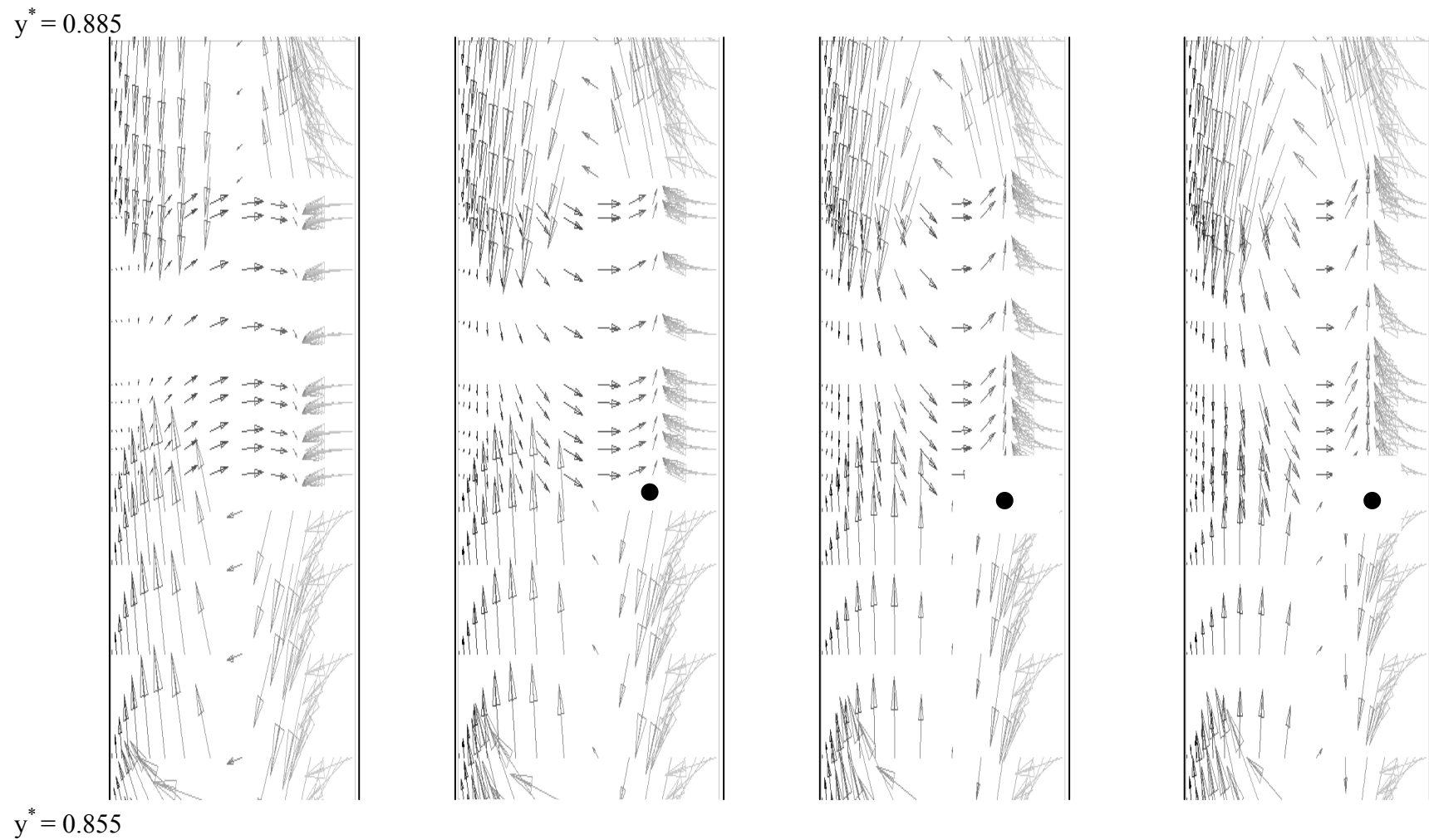


Fig. 9. Internal boundary layer formation in Taylor-Couette flow and presence of saddle point at later time for  $Re = 253$ .  
Right side indicates rotating inner wall ( $d^* = 0$ ).

the middle section of the reactor where the eddies are either very weak or not formed. All of these unsteady events would lead to an increase of mass exchange between adjacent fluid cells.

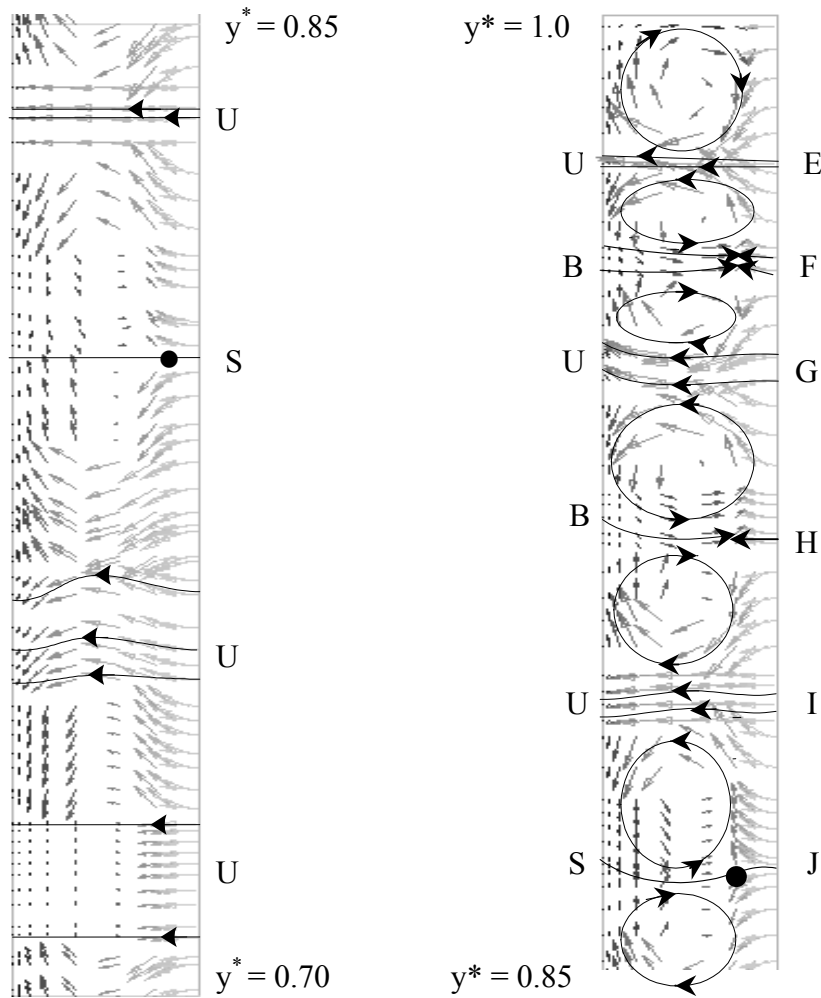


Fig. 10(a)

Fig. 10(b)

Fig. 10. Flow structure of Taylor-Couette flow for an impulsive start in supercritical regime at  $t^* = 1054$  for  $Re = 253$ . (a)  $y^*$  between 0.70 and 0.85. (b)  $y^*$  between 0.85 and 1. The notation U, B and S indicate uni-directional, bi-directional and singular flow respectively and E-J represent regions where such flows exist. Right side is rotating inner wall ( $d^* = 0$ ). • indicates a saddle point.

Finally, in this section we want to discuss about the flow structure for the chosen parameters of this computation with an impulsive start of the reactor. This aspect is very important in the context of non-unique flow evolution due to different initial conditions referred to in Andereck et al. (1986). The flow structure that we have computed is significantly different than what has been experimentally visualized by Werely and Lueptow (1998), although the geometric parameters and Reynolds number chosen are identical. This is due to the impulsive start of the present computed case as opposed to the quasi-static start in Werely and Lueptow (1998) where the inner cylinder is accelerated from rest to its final value at the very slow rate of  $0.3 Re$  per second. In Fig. 10, we show the flow structure for the two segments for  $t^* = 1054$ . The time is

not important as we have noted that the flow structure remains invariant beyond  $t^* = 575$ . We have already noted the existence of singular full saddle point in Fig. 9. If one looks carefully in Fig. 10, then one notices the jet-like flow structure between fluid cells. For example, in Fig. 10(b) the portions marked by E, G and I are the region where one can notice an unidirectional jets emerging from the inner wall and approaching the outer wall. This is the expected jet structure indicated in the sketch of Fig. 2(c). However, one can also notice the existence of bi-directional jets as marked by F and H. A longer segment originating from the outer wall and moving towards the inner wall is met with a smaller segment where the flow is from the inner to outer wall. Then, we have marked a line J in the figure, which is the limiting case of the bi-directional jet when the width of the jet degenerates into a line and the merger line of the opposing jet becomes the saddle point. The notation U, B and S in the figure indicate locations of uni-directional, bi-directional and singular zones.

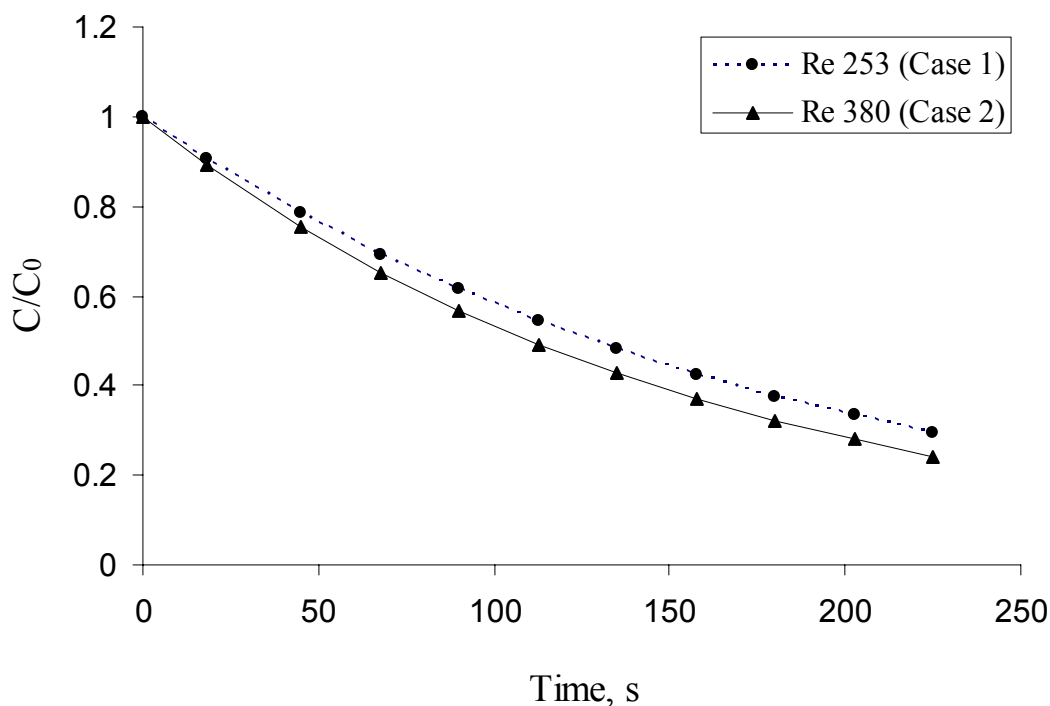


Figure 11. Photocatalytic degradation of benzoic acid.

## 5.1 PHOTOCATALYTIC REACTIONS

To analyze the performance of the TVR, benzoic acid is considered as typical pollutant present in water with an initial concentration of 100 ppm. Pollutant degradation as integrated over the full reactor volume and is shown as function of time in Fig. 11. It is to be noted that after 225s of operation, benzoic acid is degraded by about 69% and 76% respectively for case 1 ( $Re = 253$ ) and case 2 ( $Re = 380$ ). It clearly indicates the role of Taylor-Couette vortices in enhancing the rate of pollutant degradation. At early times the very rapid rate of degradation is due to the vortices that are form at the fixed ends where strong recirculating zones causes rapid mass transfer from inner to outer cylinder and back. Fig. 11 illustrates that photocatalytic reaction is diffusion controlled, as the rate of degradation increases when  $Re$  is increased. Since in this case the vortices move faster towards center from the end caps and the magnitude of the vortices are also larger compared to when  $Re = 253$ . In Fig. 12, the pollutant mass fraction contours are shown at  $t = 30s$  for photocatalytic degradation of benzoic acid for case 2. A close scrutiny of Figs. 3-10, explains the mass fraction contour plots of pollutants in Fig. 12. It reveals that reaction is faster at either

end where well-developed vortices are present while the degradation rates are slower where Taylor-Couette vortices are not well formed. The reaction takes place only in the shear layer of the inner cylinder where there are no Taylor-Couette vortices present. Figs. 11-12 clearly indicate the role of Taylor-Couette vortices in enhancing the rate of pollutant degradation. Moreover, the figures also indicate the possibility of operating the reactor in the transient mode by periodically switching the reactor on and off since during the transient phases the reaction proceed at a rapid rate due to the vortices near the end walls. Table 2 compares the performance of a slurry reactor (Mehrotra et al., 2002) with that of the two cases of Taylor vortex reactor (TVR) considered in this work for photocatalytic degradation of benzoic acid. The table clearly illustrates that increase in efficiency of TVR over the slurry reactor. One can observe 50.4% and 78.3% increase in efficiency for Taylor vortex reactor with  $Re = 253$  and with  $Re = 380$  respectively over a slurry reactor.

Table 2. Comparison of performance of Taylor vortex reactor (TVR) with that of a slurry reactor (SR) for photocatalytic degradation of benzoic acid.

	Slurry Reactor (SR)	Taylor vortex reactor (TVR)	
	Mehrotra et al., 2002	Case 1	Case 2
Volume of reactor, litre	0.0635	3.65	3.65
Catalyst surface area, $\text{cm}^2$	37000	1160	1160
‡ ICD, $\kappa$ , $\text{cm}^2/\text{cm}^3$	61.39	1.02	1.02
Volume of liquid treated, litre	0.25	1.136	1.136
Electrical energy input, W	125	30	30
Time for 50% conversion, min	3.5	2.13	1.8
§ Efficiency, $\text{h}^{-1} \text{litre}^{-1} \text{kW}^{-1}$	274	413	489
% increase in efficiency	0	50.6	78.3

‡ Illuminated catalyst density defined as illuminated catalyst surface area ( $\text{cm}^2$ ) per unit volume of liquid treated ( $\text{cm}^3$ ) in the reactor [see Ray and Beenackers, 1998].

§ Efficiency is defined as 50% pollutant (benzoic acid) converted per unit time (h) per unit volume of liquid treated (litre) per unit electrical energy input (kW).

## 6. CONCLUSIONS

A complete analysis has been performed for a heterogeneous photocatalytic Taylor vortex reactor that uses flow instability to recirculate fluid continually from the vicinity of the rotating inner cylindrical surface (coated with  $\text{TiO}_2$  catalyst) to the stationary outer cylindrical surface of an annulus. A comprehensive time accurate computation when the reactor is started impulsively shows the different stages of flow evolution and the effects of finite length of the reactor in creating eddies, the overall effects of which shows very high efficiency of photocatalytic conversion. The physical arrangement considered is such that pollutant degradation is maximized by a combination of the periodic illumination effect and the motion of fluid particles in a specific regime of centrifugal instability. It was found out that optimum Reynolds's number is around 380 as the system reaches steady state faster, number of vortices per unit length is more, vortices move faster towards center from end, and the magnitude of both axial and radial component of velocity is more than at higher or lower value of Reynolds's number. The performance of the reactor was compared with slurry reactor and it was found that efficiency of the reactor defined as conversion per unit time per unit electrical energy used per unit volume of liquid treated can be improved by 78% over a slurry reactor.

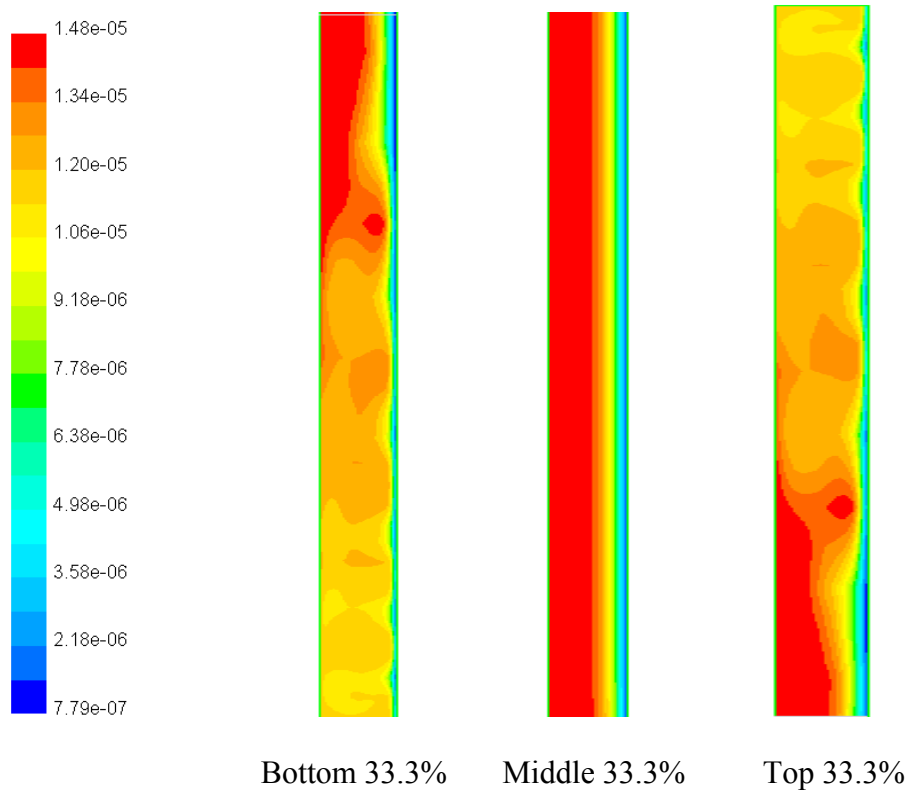


Fig 12. Contours of the mass fraction of benzoic acid in the photocatalytic reactor at  $t = 30$ s. The scale of pollutant concentration is shown on the left [ $1.5 \times 10^{-5} = 100$  ppm].

#### NOTATION

AR	aspect ratio [-]
d	annular gap, m
L	length, m
r	radius, m; radial direction, m
Re	Reynolds number [-]
t	time, s
$t^*$	Dimensionless time $\equiv t (\Omega r_i)/d$
Ta	Taylor number [-]
V	velocity, m/s
y	axial direction, m

#### Symbols

$\delta$	boundary layer thickness, m
$\kappa$	illuminated catalyst density, $\text{m}^2/\text{m}^3$
$\Omega$	rotation rate, rad/s
$\rho$	density, $\text{kg}/\text{m}^3$
$\nu$	kinematic viscosity, $\text{m}^2/\text{s}$

#### Subscripts/Superscripts

i	inner
o	outer

**REFERENCES**

- Andereck, C. D., Liu, S. S. and Swinney, H.L., "Flow regimes in a circular Couette system with independently rotating cylinders", *J. Fluid Mech.*, Vol. 164, 155-163 (1986).
- Chandrasekhar, S., "Hydrodynamics and hydromagnetic stability", Oxford University Press, Oxford, p273-340, (1961).
- Chen, D. W., Li, F. and Ray, A. K., "Effect of mass transfer and catalyst layer thickness on photocatalytic reaction", *AIChE J.*, Vol. 46, No. 5, 1034-1045 (2000).
- Chen, D. W. and Ray, A. K., "Removal of toxic metal ions from wastewater by semiconductor photocatalysis", *Chem. Eng. Sci.*, Vol. 56, No. 4, 1561-1570 (2001).
- Fox, M.A. and Dulay, M. T., "Heterogeneous photocatalysis", *Chem. Rev.*, Vol. 93, 341-352 (1993).
- Halmann, M.M., "Photodegradation of water pollutants", CRC Press, New York, (1995).
- Hermann, J. M., "Heterogeneous photocatalysis: An emerging discipline involving multiphase systems", *Catal. Today*, Vol. 24, 157-165 (1999).
- Hoffmann, M.R., Martin, S.T., Choi, W. and Bahnemann, D.W., "Environmental applications of semiconductor photocatalysis", *Chem. Rev.*, Vol. 95, 69-86 (1995).
- Ollis, D. F., Pelizzetti, E. and Serpone, N., "In Photocatalysis: Fundamentals and Applications", Edited by Serpone N. and Pelizzetti E., Wiley Interscience, New York, p603-634 (1989).
- Mehrotra, K., Yablonsky, G. and Ray, A. K., "Kinetic studies of photocatalytic degradation in TiO<sub>2</sub> slurry system: Distinguishing working regimes, Submitted to *Ind. Engg. Chem. Res.*, (2002).
- Mukherjee, P. S. and Ray, A. K., "Major challenges in the design of a large-scale photocatalytic reactor for water treatment", *Chem. Engg. Technol.*, Vol. 22, 253-260 (1999).
- Periyathamby, U. and Ray, A. K., "Computer simulation of a novel photocatalytic reactor using distributive computing", *Chem. Eng. Technol.*, Vol. 22, 881-888 (1999).
- Ray, A. K. and Beenackers, A. A. C. M., "Novel swirl-flow reactor for kinetic studies of semiconductor photocatalysis", *AIChE J.*, Vol. 43, No. 10, 2571-2578 (1997).
- Ray, A. K. and Beenackers, A. A. C. M., "Novel photocatalytic reactor for water purification", *AIChE J.*, Vol. 44, No. 2, 477-483 (1998).
- Ray, A. K., "Design, development and experimentation of a new photocatalytic reactor for water treatment", *Chem. Eng. Sci.*, Vol. 54, No. 16, 3113-3125 (1999).
- Rayleigh, L., "On the dynamics of revolving fluids", *Scientific papers*, Cambridge, England, Vol. 6, 447-458 (1920).
- Szzechowski, J.G., Koval, C.A. and Noble, R. D., "A Taylor vortex reactor for heterogeneous photocatalysis", *Chem. Eng. Sci.*, Vol. 50, No. 20, 3163-3169 (1995).
- Sengupta, T. K., Kabir, M. F., and Ray, A. K., "A Taylor vortex photocatalytic reactor for water purification", *Ind. Eng. Chem. Res.*, Vol. 40, 5268-5281 (2001).
- Taylor, G. I., "Stability of a viscous liquid contained between two rotating cylinders, *Phil. Trans. R. Soc.*, A Vol. 223, 289-297 (1923).

Werely, S. T. and Lueptow, R. M., "Spatio-temporal character of non-wavy and wavy Taylor Couette flow", *J. Fluid Mech.*, Vol. 364, 59-67 (1998).